



Corrosion and electrochemical behaviors of 7A09 Al–Zn–Mg–Cu alloy in chloride aqueous solution

Kun ZHOU^{1,2}, Bin WANG², Yu ZHAO¹, Jie LIU²

1. School of Reliability and System Engineering, Beihang University, Beijing 100191, China;
2. Southwest Technology and Engineering Research Institute, Chongqing Engineering Research Center for Environmental Corrosion and Protection, Chongqing 400039, China

Received 29 October 2014; accepted 2 April 2015

Abstract: The corrosion and electrochemical behaviors of 7A09 Al–Zn–Mg–Cu alloy were investigated in 3.5% NaCl (mass fraction) solution using complementary techniques such as scanning electron microscopy (SEM), metallographic microscopy and electrochemical measurements. The results show that both pitting corrosion from or around the intermetallic particles and intergranular corrosion are observed after the immersion test due to the inhomogeneous nature of the microstructure of the 7A09 alloy. The preferential dissolution of the anodic Cu-depleted zone along grain boundaries is believed to be the possible cause of intergranular corrosion. The passivation and depassivation of this alloy show significant dependence of immersion time, owing to the formation and dissolution of various passive films on the sample surfaces. Furthermore, the corrosion process and corrosion mechanism were also analyzed.

Key words: 7A09 Al–Zn–Mg–Cu alloy; intergranular corrosion; intermetallic particles; electrochemical impedance spectroscopy; polarization

1 Introduction

7A09 alloy belongs to the 7xxx series (Al–Zn–Mg–Cu) aluminum alloys that have excellent combination of properties such as high specific strength, fracture toughness and thermal conductivity. The superior properties of this aluminum alloy make it an ideal material for aerospace and automotive applications. This material can reach its peak strength through proper T6 aging treatment [1,2].

It has been acknowledged that corrosion resistance of aluminum alloy depends on the formation of passive film on its surface [3,4]. However, halide ions, especially chloride ions (Cl^-), show a strong attack to this passive film. The adsorption of Cl^- into the faults in the protective film, and their penetration and accumulation in these imperfections are considered one of the triggering factors of the process of nucleation of pitting [5,6]. Pitting corrosion is thought to be one of the principal mechanisms for the damage of high-strength aluminum alloys, which often represents the initiation

sites for other forms of corrosion. As pits grow, they often develop into intergranular corrosion (IGC), resulting from the existence of a continuous anodic path at grain boundaries. When a fibrous structure exists as a consequence of cold working, the voluminous expansion of the corrosion products can lead to a layered appearance, known as exfoliation corrosion [7,8]. Intergranular corrosion is usually caused by the precipitation of second-phase precipitates at the grain boundary [9,10]. During precipitation, an adjacent denuded zone free of precipitates (PFZ) is formed, which has different solution potentials compared with the matrix. The degree of susceptibility of an alloy to intergranular corrosion depends on its microstructure, in particular, the amount, size and distribution of intergranular precipitates, and the composition and the width of the PFZ.

In the past several decades, many researchers [2,11,12] have paid attention to 7A09 alloy, especially in terms of its manufacturing and deformation behavior. However, the corrosion behavior of this kind of material has seldom been studied and mentioned to our

knowledge, and the passivation and corrosion phenomena of which have not been fully understood yet. In this work, the electrochemical behavior of this alloy was evaluated in 3.5% NaCl solution using electrochemical impedance spectroscopy (EIS) and potentiodynamic techniques. Furthermore, the microstructures of the pitting attack of this alloy were investigated by metallographic microscope and scanning electron microscope (SEM), and the corrosion mechanism was also discussed.

2 Experimental

2.1 Materials and solution

A commercial T6-tempered 7A09 alloy was used in this work with the following chemical composition (mass fraction): 5.80% Zn, 2.80% Mg, 1.49% Cu, 0.23% Cr, 0.45% Fe, 0.06% Si, 0.02% Ti and balance of Al [13]. For T6 temper, the specimens were first solution annealed and then heated at 120 °C for 24 h. Before treatment. The sample surfaces were abraded with a series of silicon carbide papers, rinsed with distilled water and degreased in acetone. For electrochemical measurements, the metal samples were embedded in epoxy resin, leaving a geometrical surface area of 1 cm² exposed to the electrolyte.

As the aggressive medium, a naturally aerated and stagnant solution of 3.5% NaCl (mass fraction) at pH 8.1 was used. The saltwater was prepared from analytical grade reagents using double distilled water, and the pH of the solution was adjusted with a little strong NaOH.

In order to observe the surface corrosion morphology of the samples, the corrosion products were eliminated by immersing the samples in 70% HNO₃ for 2 min and then washed with plenty of distilled water.

2.2 Electrochemical measurement

The electrochemical measurements were performed using a conventional three-electrode cell at room temperature on a PARSTAT 2273 workstation. The cell assembly consisted of 7A09-T6 alloy as the working electrode, a platinum sheet as a counter electrode, and a saturated calomel electrode (SCE) as a reference electrode, which was connected to the corrosion solution through a Luggin capillary bridge.

Electrochemical impedance spectrum (EIS) was measured with a perturbation amplitude of 10 mV with respect to the open circuit potential (OCP) and the frequency range was from 100 kHz to 10 mHz. The EIS tests were conducted from high frequency to low frequency, and ZSimpWin 3.2 software was used for the data fitting of impedance spectra.

The potentiodynamic polarization curves of the samples in each period of immersion time of 0.5, 12, 72

and 192 h were recorded in the applied potential range from -0.4 to 1.0 V (vs SCE) with a scan rate of 1 mV/s.

2.3 Surface characterization

The optical microscope studies were conducted with a Nikon Optiphot metallographic microscope equipped with a CCD camera (Sony model Iris) connected to a computer. The samples were mechanically ground to 1500 grit SiC paper, polished with 1.5 μm diamond paste, and then etched in the solution (2 mL HF + 3mL HCl + 5 mL HNO₃ + 190 mL H₂O) for 20 s to distinguish the grain boundary for morphology observation.

The surface appearance observation of the samples was conducted with a JEOL 820-SM scanning microscope equipped with a LINK AN-10000 dispersive energy analyzer. Finally, energy dispersed spectrometry (EDS) analysis was performed during SEM observation to study the intermetallic particle composition of the samples after the immersion time of 360 h.

3 Results and discussion

3.1 Microstructure examination

Figure 1 shows the optical micrograph of 7A09-T6 aluminum alloy. From Fig. 1, it can be observed that the microstructure of the alloy in peak-aged condition (T6 tempered) is very heterogeneous, containing Al matrix, coarse intermetallic particles (constituent particles) and strengthening particles. Constituent particles (mainly FeCrAl₇, FeAl₃ and Mg₂Si) [14] are formed during casting and ingot homogenization due to the interaction between alloying elements and impurities present in the alloy.

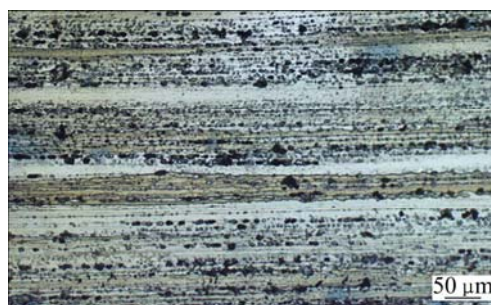


Fig. 1 Optical micrograph showing microstructure of 7A09-T6 aluminum alloy

Hardening particles, such as $T(\text{AlZnMgCu})$, precipitate in the matrix during aging treatments and provide high strength performance of the alloy. Precipitation occurs first at grain boundaries, where nucleation is easier, giving rise to the formation of grain boundary precipitates with very short interparticle distance [14]. On both sides of the grain boundaries, a narrow region where matrix is depleted in Cu has been

reported [15], leading to the so-called precipitate free zone (PFZ). In corrosive environments, the existence of these electrochemically differentiated zones gives rise to localized corrosion phenomena.

3.2 Electrochemical measurements

3.2.1 Potentiodynamic polarization curves

Figure 2 presents the potentiodynamic polarization curves for 7A09-T6 alloy in 3.5% NaCl solution after different immersion periods. It is found that the corrosion potential shifts to more noble values with the increase in immersion time. For the potentiodynamic polarization curves at immersion time of 0.5 and 72 h in solution, neither a passive current plateau nor a pitting potential is defined, indicating that active corrosion processes take place. Namely, the dissolution potential takes a value close to corrosion potential. Recent investigations [16], performed with microcells in regions free of intermetallic particles of high resistance Al alloys, have shown that the pitting potentials of these regions were much higher than those associated with particles-bearing regions. It is proposed that the observed anodic behavior is mainly due to the activity within the intermetallic particles and at their vicinity.

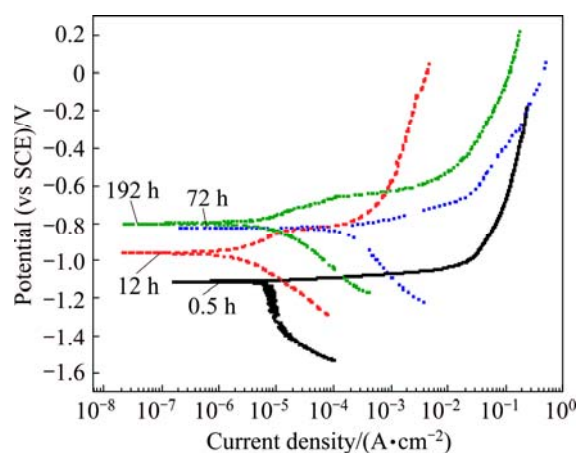


Fig. 2 Potentiodynamic polarization curves of 7A09-T6 alloy immersed in 3.5% NaCl solution as function of immersion time

In the case of the polarization curves obtained after 12 and 192 h of immersion, a passive range is established, which decreases and becomes ill-defined as immersion time increases. This response would be associated to the bulk passive alloy due to the formation of various protective compounds or corrosion products on the sample surfaces [17], as presented in Fig. 3, which reveals the existence of thick corrosion product film containing many microcracks. Corrosion products lead to the isolation of long corrosion defects from the electrolyte and to the minimization of the electrochemical processes. The accumulation of corrosion products inside the corrosion defects is

perceived as the corrosion defects healing and contributed, with the oxide film formed on the sample surfaces.

It can also be seen that, for longer immersion time, the film breakdown potential or pitting potential shifts to more noble values, suggesting that the protective layer composition changes, since the ϕ_{pit} value depends only on the passive film composition [18]. The above results also suggest that the passivation and depassivation mechanisms are related to the immersion time.

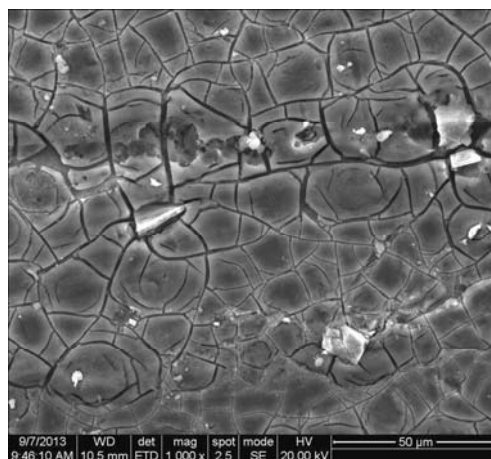


Fig. 3 SEM image of 7A09-T6 alloy sample showing corrosion product film formed after immersion in 3.5% NaCl solution for 168 h

3.2.2 Electrochemical impedance spectroscopy (EIS)

The experimental results of EIS testing are shown in Fig. 4, together with a representative fitting of a selected diagram. The plots at the immersion time of 48, 72 and 96 h present one depressed semicircle from high to medium frequencies and an inductive loop at low frequencies, and the equivalent circuit for simulating this process is shown in Fig. 5(b). It has been documented that the inductive behavior is more likely promoted by the weakening of the aluminum oxide layer due to the

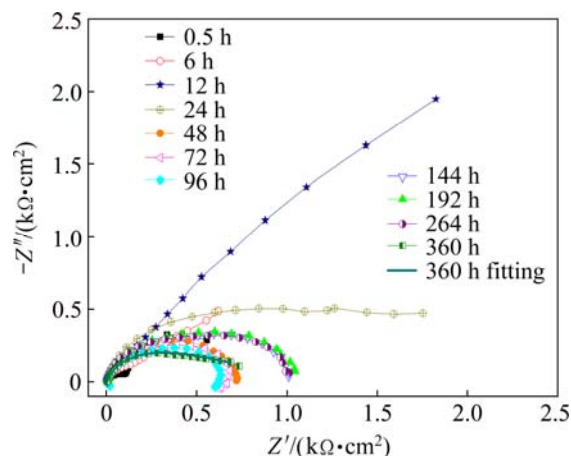


Fig. 4 Nyquist plots for samples of 7A09-T6 alloy immersed in 3.5% NaCl solution for different immersion of time

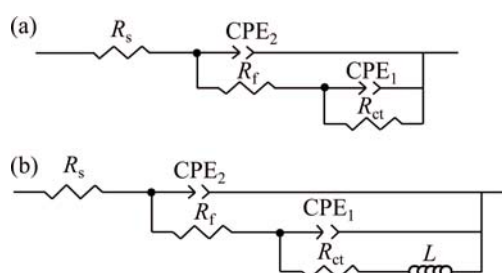


Fig. 5 Corresponding equivalent circuits used in modeling of electrochemical impedance spectrum data: (a) Before 48 h and beyond 96 h; (b) 49–96 h

anodic dissolution of aluminum alloy [19]. With increasing immersion time, the surface oxide layer becomes progressively less and less protective, due to the action of aggressive anions of the test solution. Then, the relaxation of weak points becomes vanishingly small. This is the reason that the inductive loop vanishes with the immersion period in agreement with experimental observations.

It seems that all the other Nyquist plots except 0.5 h are composed of a depressed semicircle, which may be the superimposition effect. Similar Nyquist plots for aluminum alloys were observed in the work of ZHOU et al [20] and OSORIO et al [21]. With the objective of performing accurate analysis of the EIS time-dependent constants of the corrosion process, an equivalent circuit in Fig. 5(a) has been used, which has already been proven to be a adequate choice [22,23]. The values of elements in the equivalent circuit can be defined as follows: R_s is the solution resistance, R_f is the film resistance with constant phase element CPE_2 and R_{ct} is the charge transfer resistance with constant phase element CPE_1 [24].

The simulation values analyzed by ZSimpWin software for the equivalent elements are obtained. Figure 6 summarizes the time dependence of open circuit potential (OCP), R_{ct} , R_f and CPE_1 for 7A09-T6 alloy in 3.5% NaCl solution. As seen in Fig. 6(a), at the early stage of immersion, the open circuit potential shifts to anodic values until reaching steady state. This evolution of OCP is attributed to the dissolution of aluminum and the formation of the protective oxide [25,26], which is also the reason for the sharp increase in R_f and R_{ct} values with the increase in immersion time up to 12 h, indicating a much less intense corrosion process. It is reasonable to believe that the increase in the thickness of the oxide layer leads to the decrease of the interface capacitance during the first 12 h of immersion.

However, at the immersion time of 48, 72 and 96 h, the charge transfer and film resistances (R_{ct} and R_f) exhibit low values. This result implies that the passivation is not found. The breakdown of the passive

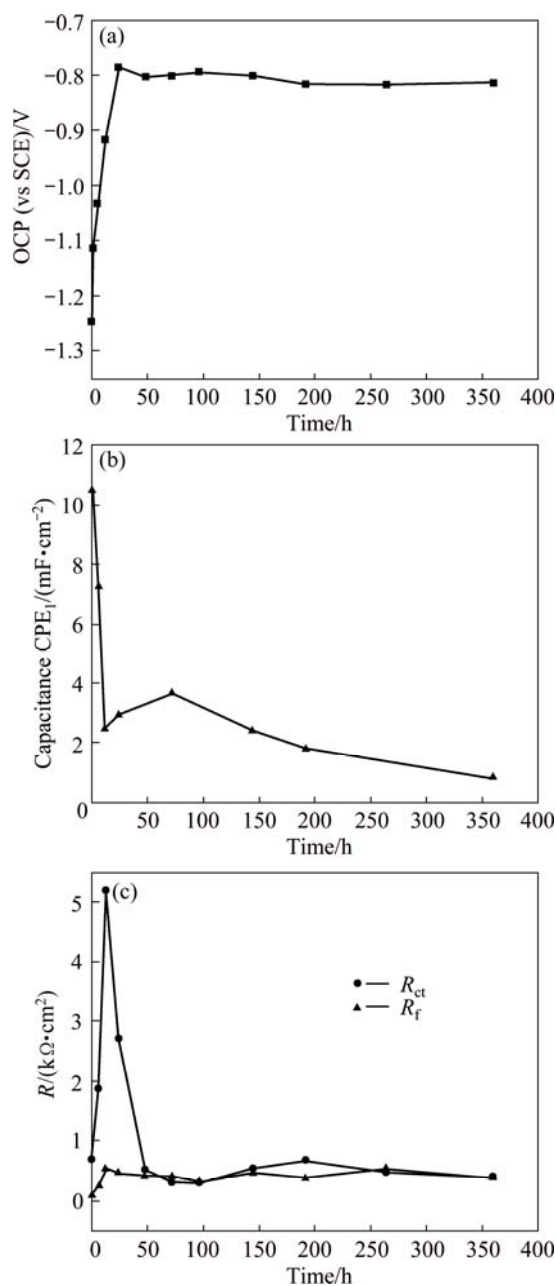


Fig. 6 Evolution of electrochemical parameters: (a) Open circuit potential (OCP); (b) Low frequency capacitance; (c) R_{ct} and R_f values for 7A09-T6 alloy samples in 3.5% NaCl solution as function of immersion time

state of aluminum and its alloys in a chloride medium occurs by the interaction between $Al(OH)_3$ film and Cl^- ions which can generate $AlCl_3$ compound [27–29] after surface saturation with corrosion products in chloride confined environments and after sufficiently long time. The values of the capacitance CPE_1 are unusually high, reaching up to 0.82–10.50 mF/cm^2 during the whole immersion time. This capacitance can be explained by the formation of the intergranular or exfoliation corrosion feature [30]. With further increase in immersion time, both R_f and R_{ct} increase slightly again,

but the values are much lower than those of the samples during the first 24 h of immersion. This direction of change is attributed to the formation of corrosion product film, but the film is less compact and corrosion resistant than that formed on sample surfaces earlier, which is due to the difference in composition of the films. These results support those observed by the potentiodynamic polarization curves as shown in Fig. 2.

3.3 Morphology of attack

SEM images of the samples immersed in 3.5% NaCl solution for different immersion time are shown in Fig. 7. The results show that pitting corrosion can be seen easily after immersion for 24 h in Fig. 7(a), and the number and size of pits increase with prolonging the soaking time. After 360 h of immersion, the sample is heavily corroded, with localized corrosion occurring in the zones at or surrounding particular types of intermetallic compounds. This type of attack leads to the formation of large numbers of mud structures and pits, which extends to cover a large proportion of the exposed surface area over prolonged periods of exposure.

The susceptibility of aluminum alloys to pitting corrosion and other forms of localized corrosion is associated with the electrochemical nature of the intermetallic phases. Thus, its corrosion behavior is often

correlated with the difference in potential between the matrix and the intermetallic compounds present in the alloy [31–33]. Anodic intermetallic particles, such as Mg_2Si , have been found to be common sites for pits nucleation. By a different process, Fig. 7(c) shows the evidence of localized dissolution of the aluminum matrix around intermetallic particles. Local compositional analysis using EDS of the corresponding regions in Fig. 7(c) confirms the presence of Al_3Fe intermetallic particles, as shown in Fig. 7(d). Furthermore, the presence of oxygen in the EDS, together with the type of corrosion displayed in the neighbouring aluminum matrix, tends to confirm the cathodic character of the Al_3Fe particles. Thus, the process of reduction of O_2 to OH^- takes place on these particles, leading to a local increase in pH in the solution adjacent to intermetallic particles. The local alkalization results in the dissolution of the layer and Al matrix surrounding the cathodic particles, while the inclusions themselves remain inert.

Figure 8 shows optical micrograph of corrosion defects for 7A09-T6 sample after 360 h of immersion. Cross-sectional view of Fig. 8 reveals that the 7A09-T6 alloy is susceptible to intergranular corrosion (IGC) and the intergranular attack tends to follow the rolling direction. Furthermore, exfoliation corrosion was not observed.

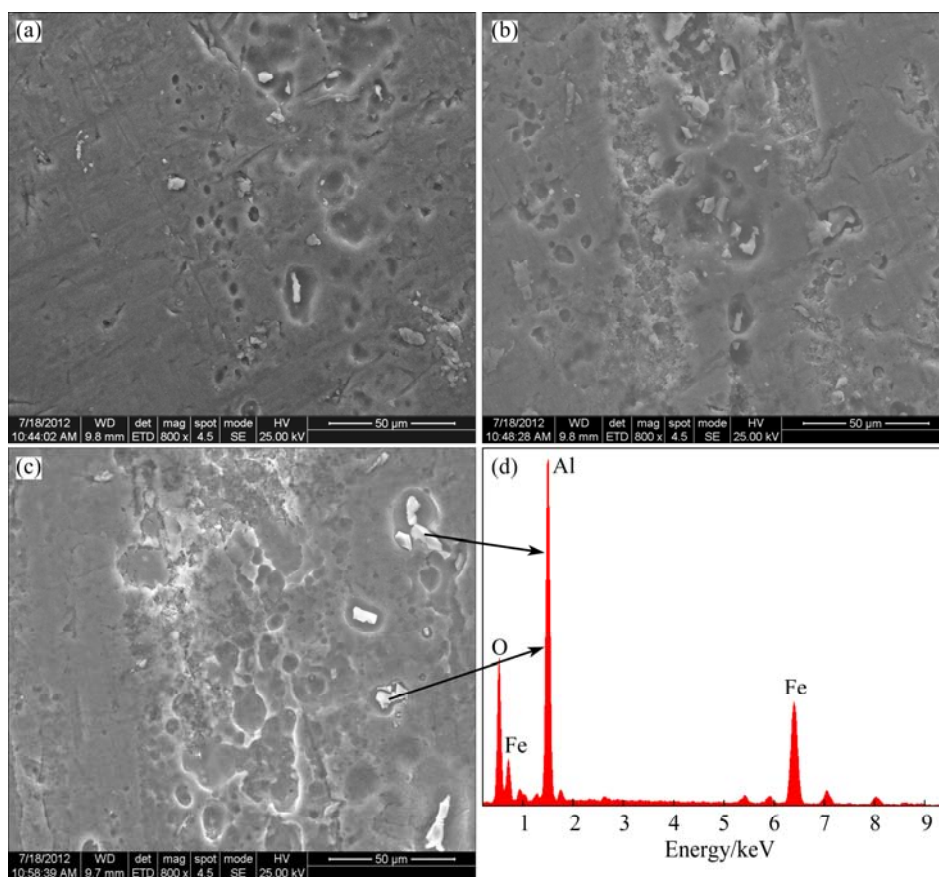


Fig. 7 SEM images of samples immersed in 3.5% NaCl solution for different immersion time: (a) 24 h; (b) 144 h; (c) 360 h; (d) EDS spectrum corresponding to representative intermetallics of Al_3Fe from 7A09-T6 sample

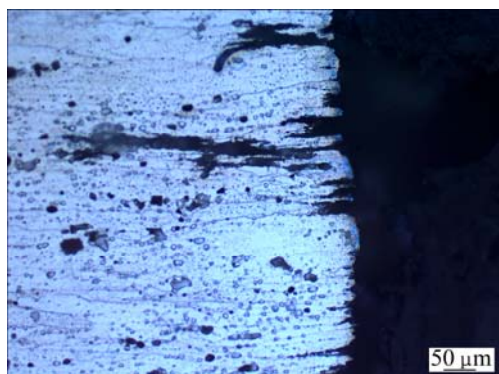


Fig. 8 Optical micrograph of corrosion defects for 7A09-T6 specimen after immersion in 3.5% NaCl solution for 360 h

It is hypothesized that IGC will initiate when a pit or localized corrosion around an intermetallic particle grows to reveal a susceptible grain boundary. For a short immersion time, the cathodic reaction was primarily oxygen reduction on the sample surface, whereas the anodic reaction was the dissolution of aluminum inside the corrosion defects. When the corrosion propagated, the accumulation of corrosion products inside the corrosion defects inhibited diffusive convection between the outside and inside of these defects to form the occluded cell corrosion. With increasing the metal ion and accumulation of positive charge, strong electric field was formed, attracting Cl^- into the pit to maintain charge neutrality, which generated a more aggressive solution with the combined effect of H^+ and Cl^- .

Due to the increased aggressiveness of the electrolyte trapped inside the corrosion defects, new corrosion defects initiated, and the dissolution of grain boundaries and subgrain boundaries also occurred. Two intergranular corrosion mechanisms have been proposed in Refs. [9,34]. The first one consists of preferential dissolution of grain boundary precipitates. If the initial grain boundary precipitate is β' or β , such a particle could serve as an anodic site and dissolve preferentially. Given that such particles are relatively anodic compared with aluminum, their dissolution shifts the alloy potential in the cathodic direction, thereby diminishing the intergranular corrosion driving force. The second one consists of preferential dissolution of the PFZ along grain boundaries.

The intergranular corrosion mechanism of 7A09-T6 alloy seems to correspond to the second proposed mechanism. Indeed, the Cu-depleted zone along grain boundaries is less noble and susceptible to anodic dissolution in particular. Moreover, pitting corrosion helps intergranular corrosion to develop since intergranular corrosion nucleates on pit walls.

4 Conclusions

1) The microstructure of 7A09-T6 alloy is very

heterogeneous. This alloy contains Mg_2Si , FeAl_3 and FeCrAl_7 constituent particles. The main hardening phase is $T(\text{AlZnMgCu})$.

2) The 7A09-T6 alloy is able to be passivated and depassivated in 3.5% NaCl solution at different immersion time due to the formation and dissolution of various passive films on the sample surfaces, and the presence of AlCl_3 decreases the protective properties of the films.

3) After the immersion test, both pitting and intergranular corrosion develop in 7A09-T6 alloy. These two forms of corrosion seem to be dependent on each other since intergranular corrosion starts on pit walls and spreads from them.

4) The intergranular corrosion mechanism of 7A09-T6 alloy consists of preferential dissolution of the anodic Cu-depleted zone along grain boundaries.

References

- [1] HILL J A, MARKLEY T, FORSYTH M, HOWLETT P C, HINTON B R W. Corrosion inhibition of 7000 series aluminum alloys with cerium diphenyl phosphate [J]. *Journal of Alloys and Compounds*, 2011, 509(5): 1683–1690.
- [2] SONG Feng-xuan, ZHANG Xin-ming, LIU Sheng-dan, TAN Qi, LI Dong-feng. Exfoliation corrosion behavior of 7050-T6 aluminum alloy treated with various quench transfer time [J]. *Transactions of Nonferrous Metals Society of China*, 2014, 24(7): 2258–2265.
- [3] SUDIC S, RADOSEVIC J, SMOLJKO I, KLISKIC M. Cathodic breakdown of anodic oxide film on Al and Al–Sn alloys in NaCl solution [J]. *Electrochimica Acta*, 2005, 50(28): 5624–5632.
- [4] SUDIC S, RADOSEVIC J, KR PAN-LISICA D, KLISKIC M. Anodic film growth on aluminum and Al–Sn alloys in borate buffer solutions [J]. *Electrochimica Acta*, 2001, 46(16): 2515–2526.
- [5] ALLACHI H, CHAOUKET F, DRAOUI K. Corrosion inhibition of AA 6060 aluminum alloy by lanthanide salts in chloride solution [J]. *Journal of Alloys and Compounds*, 2009, 475(1): 300–303.
- [6] BESSONE J B, SALINAS D R, MAYER C E, EBERT M, LORENZ W J. An EIS study of aluminum barrier-type oxide films formed in different media [J]. *Electrochimica Acta*, 1992, 37(12): 2283–2290.
- [7] REBOUL M C, BAROUX B. Metallurgical aspects of corrosion resistance of aluminum alloys [J]. *Materials and Corrosion*, 2011, 62(3): 215–233.
- [8] ABREU C M, CRISTOBAL M J, FIGUEROA R, PENA G. Influence of molybdenum ion implantation on the localized corrosion resistance of a high strength aluminum alloy [J]. *Corrosion Science*, 2012, 54: 143–152.
- [9] EI-AMOUSH A S. Intergranular corrosion behavior of the 7075-T6 aluminum alloy under different annealing conditions [J]. *Materials Chemistry and Physics*, 2011, 126(3): 607–613.
- [10] TIDAN U, GRUM J. SEM/EDS characterization of laser shock peening effect on localized corrosion of Al alloy in a near natural chloride environment [J]. *Corrosion Science*, 2014, 82: 328–338.
- [11] WU Xin, HAN Fei, WANG Wei-wei. Effects of solution treatment and aging process on microstructure refining of semi-solid slurry of wrought aluminum alloy 7A09 [J]. *Transactions of Nonferrous Metals Society of China*, 2009, 19(S2): s331–s336.
- [12] WANG Wei-wei, JIA Bin-bin, LUO Shou-jing. Effect of heat treatment on mechanical properties of thixoformed 7A09 aluminum alloy [J]. *Transactions of Nonferrous Metals Society of China*, 2009,

- 19(S2): s337–s342.
- [13] JI H Z, YUAN L, SHAN D B. Effect of microstructure on thermal expansion coefficient of 7A09 aluminum alloy [J]. Journal of Materials Science and Technology, 2011, 27(9): 797–801.
- [14] YAN Ming-gao. China aeronautical materials handbook [M]. 2nd ed. Beijing: China Standard Press, 2001: 210–218. (in Chinese)
- [15] MENG Q, FRANKEL G S. Effect of Cu content on corrosion behavior of 7xxx series aluminum alloys [J]. Journal of the Electrochemical Society, 2004, 151(5): 271–283.
- [16] QUEIROZ F M, MAGNANI M, COATA I, de MELO H G. Investigation of the corrosion behavior of AA 2024-T3 in low concentrated chloride media [J]. Corrosion Science, 2008, 50(9): 2646–2657.
- [17] LIU J, ZHU X Y, SUDAGAR J, DIAO W, YU S. Increased corrosion resistance of closed-cell aluminum foams by electroless Ni-P coatings [J]. Materials Transactions, 2011, 52(12): 2282–2284.
- [18] ARRABAL R, MINGO B, PARDO A, MOHEDANO M, MATYKINA E, RODRIGUEZ I. Pitting corrosion of rheocast A356 aluminum alloy in 3.5 wt.% NaCl solution [J]. Corrosion Science, 2013, 73: 2646–2657.
- [19] KRISHNA GOPALA K, SIVAPRASAD K, SANKARA NARAYANAN T S N, HARI KUMAR K C. Localized corrosion of an ultrafine grained Al-4Zn-2Mg alloy produced by cryorolling [J]. Corrosion Science, 2012, 60: 82–89.
- [20] ZHOU H R, LI X G, MA J, DONG C F, HUANG Y Z. Dependence of the corrosion behavior of aluminum alloy 7075 on the thin electrolyte layers [J]. Materials Science and Engineering B, 2009, 162(1): 1–8.
- [21] OSORIO W R, FREITAS E S, GARCIA A. EIS and potentiodynamic polarization studied on immiscible monotectic Al-In alloys [J]. Electrochimica Acta, 2013, 102: 436–445.
- [22] DU Xiao-qing, YANG Qing-song, CHEN Yu, YANG Yang, ZHANG Zhao. Galvanic corrosion behavior of copper/titanium galvanic couple in artificial seawater [J]. Transactions of Nonferrous Metals Society of China, 2014, 24(2):570–581.
- [23] SHI H, HAN E H, LIU F. Corrosion protection of aluminum alloy 2024-T3 in 0.05 M NaCl by cerium cinnamate [J]. Corrosion Science, 2011, 53(7): 2374–2384.
- [24] ABALLE A, BETHENCOURT M, BOTANA F J, OSUNA R, MARCOS. Using EIS to study the electrochemical response of alloy AA5083 in solutions of NaCl [J]. Materials and Corrosion, 2001, 52(3): 185–192.
- [25] HAGYARD T, WILLIAMS J R. Potential of aluminum in aqueous chloride solutions [J]. Transactions of the Faraday Society, 1961, 57: 694–698.
- [26] KHIREECHE S, BOUGHRARA D, KADRI A, HAMADOU L, BENBRAHIM N. Corrosion mechanism of Al, Al-Zn and Al-Zn-Sn alloys in 3 wt.% NaCl solution [J]. Corrosion Science, 2014, 87: 504–516.
- [27] KAEWMANEEKUL T, LOTHONGKUM G. Effect of aluminum on the passivation of zinc-aluminum alloys in artificial seawater at 80 °C [J]. Corrosion Science, 2013, 66: 67–77.
- [28] PYUN S I, MOON S M, AHN S H, KIM S S. Effects of Cl^- , NO_3^- and SO_4^{2-} ions on anodic dissolution of pure aluminum in alkaline solution [J]. Corrosion Science, 1999, 41(4): 653–667.
- [29] KALE S S, RAJA V S, BAKARE A K. Environmentally assisted cracking behavior of Al-Zn-Mg-Cu alloy bonded with polymer matrix composite stiffener [J]. Corrosion Science, 2013, 75: 318–325.
- [30] KEDDAM M, KUNTZ C, TAKENOUTI H, SCHUSTER D, ZUILI D. Exfoliation corrosion of aluminum alloys examined by electrode impedance [J]. Electrochimica Acta, 1997, 42(1): 87–97.
- [31] BETHENCOURT M, BOTANA F G, CALVINO J J, MARCOS M, PERE J, RODRIGUEZ M A. The influence of the surface distribution of $\text{Al}_6(\text{MnFe})$ intermetallic on the electrochemical response of AA 5083 aluminum alloy in NaCl solutions [J]. Materials Science Forum, 1998, 289–292: 567–574.
- [32] ALAVI A, COTTIS R. The determination of pH, potential and chloride concentration in corroding crevices on 304 stainless steel and 7475 aluminum alloy [J]. Corrosion Science, 1987, 27(5): 443–451.
- [33] ZAMIN M. The role of Mn in the corrosion behavior of Al-Mn alloys [J]. Corrosion, 1981, 37(11): 627–632.
- [34] GUILLAUMIN V, MANKOWSKI G. Localized corrosion of 6056 T6 aluminum alloy in chloride media [J]. Corrosion Science, 2000, 42(1): 105–125.

7A09 Al-Zn-Mg-Cu 合金在氯化物溶液中的 腐蚀和电化学行为

周堃^{1,2}, 王彬², 赵宇¹, 刘杰²

1. 北京航空航天大学 可靠性与系统工程学院, 北京 100191;
2. 西南技术工程研究所 重庆市环境腐蚀与防护工程技术研究中心, 重庆 400039

摘要: 采用扫描电镜、金相显微和电化学测试等综合评价技术研究 7A09 铝合金在 3.5% NaCl(质量分数)水溶液中的腐蚀和电化学行为。结果表明: 7A09 铝合金不均一的显微组织结构导致该合金遭受严重的点蚀和晶间腐蚀, 其中点蚀主要发生于金属间化合物或其周围, 而沿晶界分布的阳极贫铜区的优先溶解是引起晶间腐蚀的主要原因。当不同浸泡时间时, 在 7A09 铝合金表面交替进行着不同钝化膜的生成与溶解过程, 并伴随着该合金钝化与去钝化行为的发生。同时, 对该合金的腐蚀过程及机制进行分析。

关键词: 7A09 Al-Zn-Mg-Cu 合金; 晶间腐蚀; 金属间化合物; 电化学阻抗谱; 极化

(Edited by Wei-ping CHEN)